Supporting Information

Ligand-induced structural changes of thiolate-capped gold nanoclusters observed with resistive-pulse nanopore sensing

Bobby D. Cox, Patrick H. Woodworth, Peter D. Wilkerson, Massimo F. Bertino and Joseph E. Reiner*

Department of Physics, Virginia Commonwealth University, Richmond, VA USA 23284

*Corresponding author: Joseph Reiner - jereiner@vcu.edu

Table of Contents *Page*

1. Methodology

1A. Nanoparticle synthesis

All chemicals were purchased from Sigma-Aldrich and used as received unless otherwise noted. Nanoparticle synthesis was carried out by reducing potassium gold (III) chloride ($KAuCl_4$) in the presence of thiolated-ligands (*p*-MBA, TP or S-PEG_7 (Polypure, Finland)) using borane *tert*-butylamine complex (BTBC).[1] The 7 subscript on the PEG indicates a monodisperse mixture with all polymers having seven repeat monomer units. Au_x(*p*-MBA)$_y$ and Au_x(TP)$_y$ clusters were synthesized in methanol while Au_x(S-PEG_7)$_y$ were formed in water.

To synthesize the *p*-MBA-capped and TP-capped particles, potassium gold (III) chloride and ligand (*p*-MBA or TP) were dissolved in separate vials of methanol at equal concentrations prior to mixing. The ligand solution was then added to the gold chloride solution and vigorously shaken for ca. 30 seconds. A premade solution of BTBC in methanol was added to the ligand-gold solution and vortexed for ca. 30 seconds. This solution was then sonicated for 20 minutes and during this time the solution would turn dark brown, indicating the formation of nanoscale clusters. The final concentrations of the $KAuCl_4$, ligand and BTBC were 1:1:5 mM respectively. Finally, the ligand-capped particle solution, in methanol, was evaporated in a fume hood overnight and rehydrated with 1 mL of water.

To synthesize the water-soluble S-PEG_7-capped particles, potassium gold (III) chloride and S-PEG_7 were dissolved in water in separate vials prior to mixing and reduced with a premade solution of BTBC. The solution was vigorously stirred for 1 min, then sonicated for 20 min until it turned brown. The final concentrations of the $KAuCl_4$, S-PEG_7 and BTBC were 1:2:5 mM respectively. The S-PEG_7 particles were synthesized in water and thus no evaporation step was necessary. No further size exclusion step was taken because the αHL nanopore does not yield any signal from particles larger than ca. 3 nm.[2]

The nanopore serves as a size filter that rejects particles larger than the pore opening (~3 nm). This means a polydisperse mixture of particle sizes may still enter into the pore. It would be ideal if one could perform high-resolution mass spectrometry on particles trapped within the pore to identify the exact makeup of each particle, but Fig. S1 below suggests this may not be necessary. Figure S1 compares the current blockade distributions from an ensemble of monodisperse particles[3] ($Au_{25}(SG)_{18}$) with the polydisperse *p*-MBA particles used throughout this report. First, the blockade depth is comparable between the two suggesting that the size of the captured *p*-MBA particles is similar to the monodisperse particles. More importantly, the

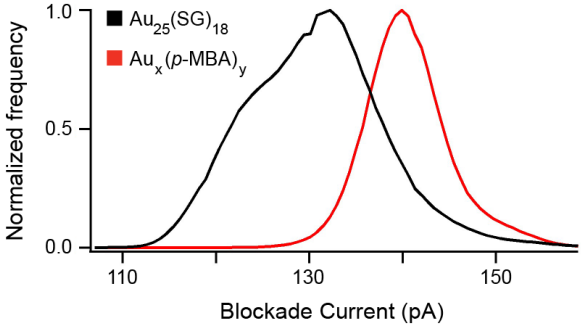

Figure S1: Similar widths for the current blockade distributions of monodisperse (black) and polydisperse (red) mixtures suggest that αHL is an efficient filter that isolates one size from our polydisperse mixtures. Experimental conditions for both distributions were identical ([KCl] = 3M, pH 7, V_{app} = 70 mV) and each distribution was normalized to a maximum value of 1. Numerous particle capture events were used to construct each distribution (N(SG) ≈ 200 and N(*p*-MBA) = 8).

width of the current blockade distribution is also similar, which suggests that the nanopore-captured *p*-MBA particles reported herein represent a monodispserse subset of the particles synthesized for analysis.

1B. Nanopore sensing

All experiments were carried out with standard techniques for single αHL nanopore sensing. The general protocol can be found elsewhere,[4] but we briefly describe our methodology here. A horizontal DPhy:PC (Avanti Polar Lipids, Alabaster, AL) bilipid membrane was formed in an electrolyte solution (3 M KCl, 10 mM TRIS at various pH) by a modified painting method.[5] The unsupported membrane spans a 50-μm hole preformed in a 20 μm thick PTFE (Teflon) partition sheet (Eastern Scientific LLC, Rockville, MD). The tip insertion method[5] was used to load a single αHL channel (List Biological Laboratories, Inc., Campbell, CA) into the bilipid membrane and this was confirmed from the expected single channel conductance of an αHL pore.[6] Alpha hemolysin exhibits a small degree of rectification[6] and this was used to confirm the proper orientation of the pore (*cis*-side facing up) in the membrane.

To guarantee that all particle fluctuations only result from a single isolated particle, rather than additional particles interacting with a cluster-occupied pore, we kept the *cis*-side solution clear by utilizing a particle ejection protocol. Briefly, a 1:4 nanoparticle:electrolyte solution was backloaded into a micropipette tip formed from a borosilicate capillary (OD = 1.0 mm and ID = 0.78). We used preset program #11 on the P-2000 puller (Sutter Instruments, Novato, CA) to form the micropipettes with a final ID of ca. 1-2 μm. The nanoparticle-containing micropipette was positioned ca. 50 micron above the membrane and 20 micron to the left edge of the membrane near the *cis*-side of the pore. A transmembrane voltage was applied (Axopatch 200B, Molecular Devices, Carlsbad, CA) with the appropriate polarity (ground held fixed on the *cis*-side of the membrane) and a backing pressure was applied (~15 hPa) (Femtojet, Eppendorf, Hauppauge, NY) to eject particles from the tip. After some time (ca. 30 s) a rapid downward spike in the current indicated the entry of a single cluster into the pore and the backing pressure was immediately reduced to zero. This created a backflow into the tip and this, along with Brownian diffusion, removed the possibility of more particles entering the pore. The voltage difference was fixed across the membrane and the current was recorded until the particle escaped from the pore. The nature of the current around the escape time (an upward transition to the open state rather than a rapid downward transition) indicates that particles usually exit the pore from the *cis*-side vestibule.

1C. Data Analysis

Current traces were measured through a 10-kHz, four-pole, low-pass Bessel filter and digitally sampled at 50 kHz (Digidata 1440A, Molecular Devices). Data was recorded as axon binary files (.abf) and stored for offline analysis. To observe the discrete current steps, we applied a fourth-order infinite impulse response (IIR) low-pass digital filter (IGOR 6.37, Wavemetrics, Portland, OR) with the low-pass frequency set to 100 Hz (1000 Hz for S-PEG$_7$-capped particles). All-points histograms were calculated with IGOR 6.37 software. Multi-level state analysis was performed with in-house software programmed in MATLAB utilizing the cumulative sums

algorithm (CUSUM) described by Raillon et al.[7] (MATLAB code available upon request). CUSUM analysis yielded the step size and step duration distributions shown in Figs. 2-3 in the main article and Figure S3 below. Figure S2 shows typical current traces and the corresponding CUSUM fitting results for all three ligands studied.

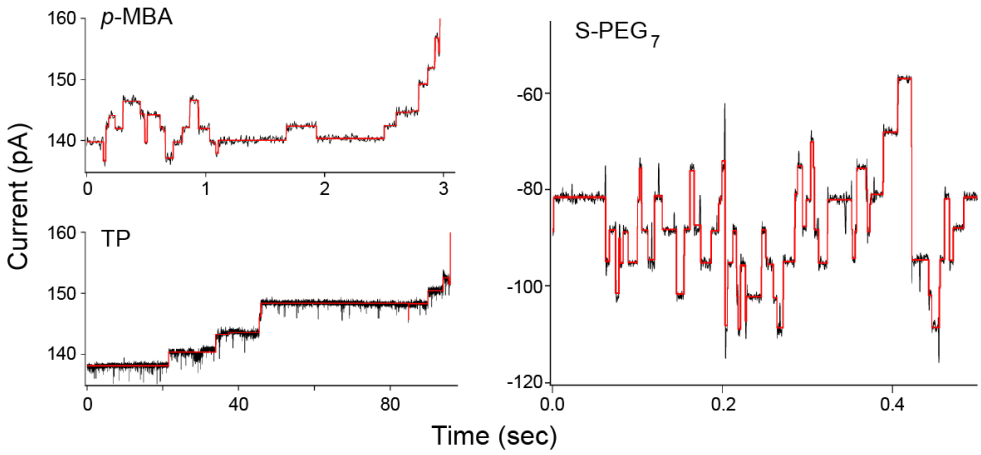

Figure S2: Typical current traces for *p*-MBA, TP and S-PEG$_7$ capped clusters (black) and CUSUM fits (red). All data shown here was collected at 70 mV in 3M KCl at pH 8.0 and filtered with 100 Hz (1000 Hz for S-PEG$_7$) low pass filter.

We note that in many of the blockade events the current tends to undergo a decay towards the open state (i.e. Figs. 1B, 3A, 3C, S2 (*p*-MBA), S2 (TP)). The exact mechanism for this decay is unknown, but we conjecture that it most likely results from the particles drifting up through the *cis*-side vestibule or from changes in the ligands through either folding, rearrangement or detachment from the cluster core.

Finally, the number of pores, clusters and current steps used to calculate the residence time and current step distributions in the main article are listed below:

Figs. 2E, 3B (*p*-MBA, pH 8) = 3 pores, 20 clusters, 718 current steps
Fig. 3D (TP, pH 8) = 3 pores, 20 clusters, 179 current steps
Fig. 3F = 2 pores, 3 clusters, 400 current steps

II. Geometric model of the cluster-induced current steps

Figure 2E from the main article shows that current steps from *p*-MBA-capped particles at pH 8 are limited to nearest neighbor and next-nearest neighbor transitions. Figure S3 below shows similar behavior for *p*-MBA particles at pH 7 and for S-PEG$_7$-capped particles as well. Tiopronin fluctuations are not reported because the limited number of current steps prevents the formation of a well-defined current step distribution. We hypothesize that current transitions are caused by changes of the ligand-cluster interface and that the location of a change, with respect to the cluster orientation within the pore, dictate the size of the corresponding current step.

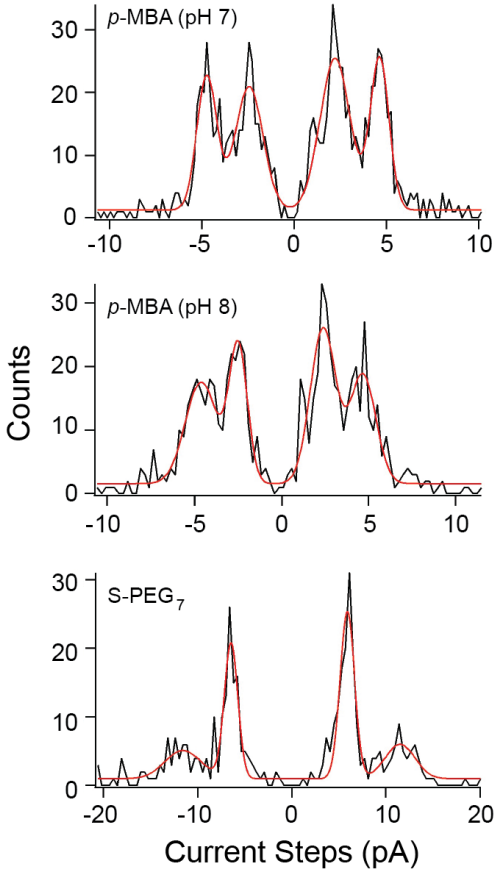

Figure S3: Current step distributions (black) for *p*-MBA at pH 7, pH 8 and for S-PEG$_7$ particles. (The pH 8 distribution is reproduced from Fig. 2E of the main article). In each case the steps show that transitions occur between nearest neighbor and next-nearest neighbor current states. This is confirmed with Gaussian mixture model fitting (red). The peak positions (± 1 S.D.) for each ligand type are listed below:

[*pH 7* = (-4.73 ± 0.05) pA, (-2.44 ± 0.06) pA, (2.21 ± 0.05) pA, (4.62 ± 0.04) pA]
[*pH 8* = (-4.63 ± 0.14) pA, (-2.50 ± 0.08) pA, (2.36 ± 0.09) pA, (4.67 ± 0.12) pA]
[*S-PEG$_7$* = (-11.6 ± 0.5) pA, (-6.49 ± 0.07) pA, (5.89 ± 0.05) pA, (11.5 ± 0.4) pA]

All data was collected under an applied 70 mV transmembrane potential in 3M KCl. Current steps were calculated using our modified CUSUM algorithm.[7] The *p*-MBA at pH 7 distribution results from 3 pores, 21 clusters and 994 current steps. The *p*-MBA at pH 8 distribution results from 3 pores, 20 clusters and 718 current steps. The S-PEG$_7$ distribution results from 2 pores, 3 clusters, and 400 current steps.

Specifically, we hypothesize that a ligand-induced geometric change along the pore axis will yield a smaller current step than a ligand-induced change perpendicular to the pore axis. In this section we support this hypothesis by developing a geometric model of the connection between changes in the cluster-ligand structure and corresponding current steps. Figure S4 shows our model representation of the pore and cluster. For simplicity, we model the pore as a right circular cylinder with length L_p and diameter D. The cluster is modelled as a sphere of diameter d located at the center of the pore. Changes to the cluster structure are modelled by the appearance of a small cube of side length δ on the side or front face of the spherical cluster. A detailed description of the connection between ligand kinetics and structural changes to the cluster is outlined in the figure caption.

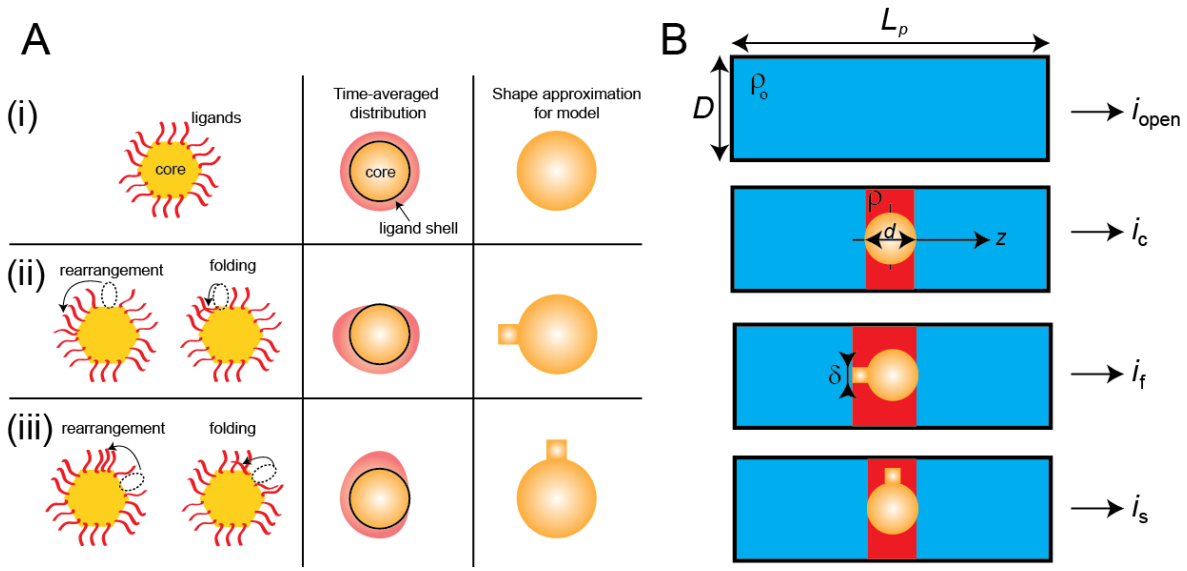

Figure S4: Schematic illustration of the geometric-model used to derive normalized current blockade values. (A) We hypothesize that ligand kinetics are the major cause of the observed current-step fluctuations. We assume these fluctuations result from either ligand folding or rearrangement on the cluster surface. (i) This in turn leads to modifications of the cluster geometry visualized with the time-averaged mass distribution. (ii) Changes to ligands on the top (or bottom) of the cluster lead to an increase in the mass density along the pore axis. (iii) Changes to ligands along the pore axis lead to distortions in the cluster mass distribution perpendicular to the pore axis. (B) The pore is modeled as a right-circular cylinder with length L_p = 6 nm, diameter D = 2.6 nm and open-pore resistivity ρ_o. An applied voltage gives rise to the open pore current i_{open}. Spherical clusters with diameter d enter the pore and reside in the center. We assume that the resistivity changes near the cluster from ρ_o to ρ and this is represented with the red shading. This gives rise to the cluster current i_c. Small steps in the current correspond to changes in cluster structure. We model these structural changes as cubes with side length δ. These cubes appear either along the front of the cluster (i_f) or on the side of the cluster

Neglecting the access resistance of the pore and utilizing the well-known relationship connecting the resistance R, resistivity $\rho(z)$ and pore geometry, $R = \int\rho(z)dz/A(z)$, where $A(z)$ is the cross-sectional area along the pore axis, z, we arrive at the following expressions for the open pore resistance,

$$R_o = \frac{4\rho_o L_p}{\pi D^2}, \tag{S1.1}$$

where ρ_o is the resistivity in the pore. The resistance with a cluster in the pore is given by

$$R_c = \frac{4\rho_o\left(L_p - d\right)}{\pi D^2} + \int_{-d/2}^{d/2} \frac{4\rho dz}{\pi D^2 - \pi d^2 + 4\pi z^2} \tag{S1.2}$$

where ρ is the resistivity in the vicinity of the cluster (see Fig. S4). The resistance with the cluster in the pore and a small cubic extension on the front face of the cluster is given by

$$R_f = R_c + \frac{4\rho\delta}{\pi D^2 - 4\delta^2} - \frac{4\rho_o\delta}{\pi D^2} \tag{S1.3}$$

and the resistance with the cluster in the pore and a cubic extension on the side face of the cluster is given by

$$R_s = R_c + \int_{-\delta/2}^{\delta/2} \frac{4\rho dz}{\pi D^2 - \pi d^2 + 4\pi z^2 - 4\delta^2} - \int_{-\delta/2}^{\delta/2} \frac{4\rho dz}{\pi D^2 - \pi d^2 + 4\pi z^2} \tag{S1.4}$$

As was previously noted,[8] these expressions give a lower bound for the resistance because the actual electric field lines within the pore are not parallel to the pore axis throughout. Nevertheless, these equations serve as an instructive tool to study the connection between cluster structure and the corresponding current measurements. Our experiments measure the relative changes in the current with the addition of the cluster to the pore and Eqs. S1.1-S1.4 can be used to connect these changes to the clusters structural change within the pore. We use Ohm's law to connect the observed currents to the resistances listed above (i.e. $\Delta V = i_o R_o = i_c R_c = i_f R_f = i_s R_s$) and assume changes in the current and resistance arise from a cluster entering the pore and undergoing structural changes within the pore. This leads to the following expression for the normalized current blockade when a spherical cluster enters the pore,

$$\frac{i_c}{i_o} = \frac{R_o}{R_c} = \left(1 + \frac{\rho}{\rho_o}\frac{D}{L_p}\frac{\sin^{-1}\left(d/D\right)}{\sqrt{1-\left(d/D\right)^2}} - \frac{d}{L_p} \right)^{-1} \tag{S1.5}$$

When the cluster remains trapped in the pore, we see small current steps that we hypothesize originate from a structural change to the cluster. From Eqs. S1.1-S1.4 we find the normalized current jump due to a geometric change on the front face of the particle,

$$\frac{\delta i_f}{i_o} = \frac{i_f - i_c}{i_o} = \frac{R_o}{R_c}\frac{R_c - R_f}{R_f} \approx \left(\frac{i_c}{i_o}\right)^2 \frac{R_c - R_f}{R_o} \approx \frac{\delta}{L_p}\left[1 - \frac{\rho}{\rho_o} - \frac{4}{\pi}\frac{\rho}{\rho_o}\left(\frac{\delta}{D}\right)^2\right]\left(\frac{i_c}{i_o}\right)^2 \tag{S1.6}$$

and the normalized current jump due to a geometric change on the side face of the particle is given by,

$$\frac{\delta i_s}{i_o} = \frac{i_s - i_c}{i_o} = \frac{R_o}{R_c}\frac{R_c - R_s}{R_s} \approx \left(\frac{i_c}{i_o}\right)^2 \frac{R_c - R_s}{R_o} \approx \left[-\frac{\rho}{\rho_o}\frac{4\delta^3}{\pi D^2 L_p}\left(1 - \left(d/D\right)^2\right)^{-2}\right]\left(\frac{i_c}{i_o}\right)^2 \tag{S1.7}$$

The analytical expressions for Eqs. S1.6 and S1.7 are cumbersome so we expanded the relative current jumps to second order in δ/D. Equations S1.5-S1.7 are all measureable parameters from the current traces and the current step distributions. These three equations contain five independent unknown parameters (d, D, L_p, ρ/ρ_o, δ), which we reduce to three parameters by fixing the known values for the pore diameter (D = 2.6 nm) and length (L_p = 6 nm).[2] This yields a completely determined system from which we can extract d, D and ρ/ρ_o.

A typical experiment with the *p*-MBA-capped ligands in pH 8 solution yields an open state current of i_o = 185 pA, a corresponding cluster-induced blockade current of i_c = 142 pA and current steps of δi_f = -2.4 pA and δi_s = -4.7 pA. Substituting these values into Eqs. S1.5-S1.7 yields a cluster size of d = 1.9 nm and a cubic fluctuation size of δ = 0.6 nm, which are both within the expected range for the cluster size (d = (1.8 ± 0.4) nm,[9] and the *p*-MBA ligand size $l_{p\text{-MBA}}$ = 0.6 nm[10]).

The known dimensions of the αHL pore along with the clearly defined current steps allow one to extract structural parameters of the clusters within the pore. Our geometric-model leads to reasonably accurate results for the expected size of the clusters and supports our hypothesis that the small current steps seen in Figs. 2 and 3 of the main article and Figs. S2 and S5 here in the SI most likely result from structural changes at the ligand-core interface. This suggests that nanopore sensing can provide a powerful tool for characterizing cluster-bound ligand kinetics.

III. pH studies of the cluster-induced kinetics

3A. Lowering pH degrades fluctuations

To rule out the possibility that the discrete steps observed in Figs. 2B,3A,3C and 3E of the main article result from protonation/deprotonation of the carboxylic acid on the end of the *p*-MBA particles, we measured current traces from numerous *p*-MBA particles under a variety of different pH conditions. Figure S5 shows typical current traces and corresponding all-points histograms from trapped *p*-MBA particles at different pH. The discrete steps can be resolved at pH > 6.5, but the kinetics of the steps appear nearly-identical at pH 7 and pH 8 (see Fig. S5I).

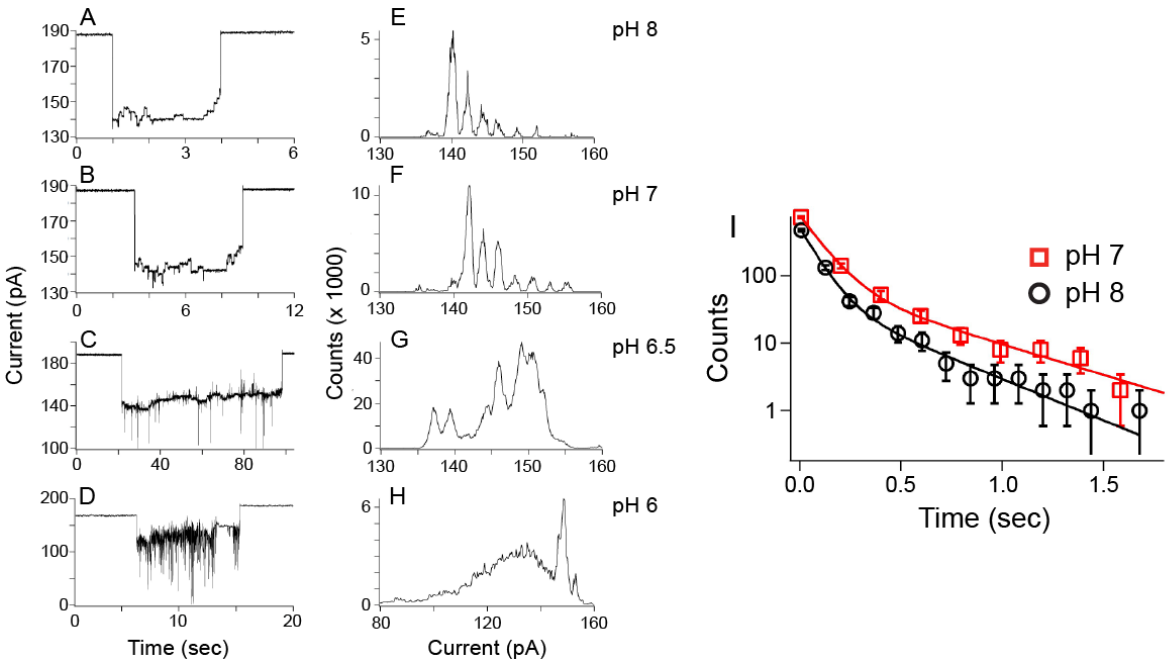

Figure S5: *p*-MBA cluster-induced fluctuations become noisier with decreasing pH, and the current step kinetics are independent of pH. (A-D) Typical single particle current traces filtered with a 100 Hz low-pass filter show that the clear steps present at high pH are lost as the pH is reduced ((A,E) = pH 8, (B,F) = pH 7, (C,G) = pH 6.5, (D, H) = pH 6). (E-H) The corresponding all-points histograms show that the current states become less resolved as the pH decreases towards the expected pK_a of the cluster bound ligands (pK_a ~ 5).[11] (I) Comparison of the step-time distributions for the pH 8 (black) and pH 7 (red) conditions shows that the discrete steps at high pH are not the result of protonation/deprotonation of the carboxylic acid groups on the *p*-MBA ligands. The solid lines are least-squares fits to the data (open squares and circles) with double exponential distributions from which we extract the following time constants: ($\tau_{pH7,\ fast}$ = (0.11 ± 0.01) s, $\tau_{pH7,\ slow}$ = (0.64 ± 0.12) s, $\tau_{pH8,\ fast}$ = (0.08 ± 0.01) s, $\tau_{pH8,\ slow}$ = (0.35 ± 0.08) s). The pH 7 residence time distribution results from 3 pores, 21 clusters, and 994 current steps. The pH 8 distribution results from 3 pores, 20 clusters and 718 current steps. Error bars correspond to ± 1 S.D. All data shown here was collected in 3M KCl under a 70 mV applied transmembrane potential.

This proves that the discrete current steps are not related to protonation-deprotonation events. Additionally, the all-points histograms of the current traces shown in Figure S4 indicate a significant degradation of the discrete current steps as the pH is lowered from pH 8 to pH 6. Below pH 6 we found that the particles crashed out in the high ionic strength solutions as expected given the reported pK_a range for these particles ($5 < pK_a < 7$).[11] This onset of excess noise with decreasing pH suggests that protonation/deprotonation kinetics create higher frequency current fluctuations than those observed in the discrete state steps. Finally, we note that the ionic strength of the NP spray for the pH 6 solution was reduced to [KCl] = 1.5M to minimize particle crash out within the NP tip. This led to a sizable difference in the open pore states before and after the particle capture.

3B. Acidic spray experiments

To better understand the rapid, pH-induced kinetics seen in Fig. S5, we performed acidic spray experiments where a single *p*-MBA particle was held fixed in the pore at pH 8 while a second micropipette tip containing an acidic electrolyte with matching ionic strength (pH 5) was intermittently sprayed onto the pore. The volume of pH 5 solution sprayed onto the pore is on the order of picoliters so when the acidic-spray is stopped, the pH inside the pore quickly returns to pH 8. Figure S6 shows a typical result where the presence of the acidic solution yields a large number of short downward spikes whose duration is exponentially distributed with mean times of (29 ± 2) μs and (98 ± 16) μs.

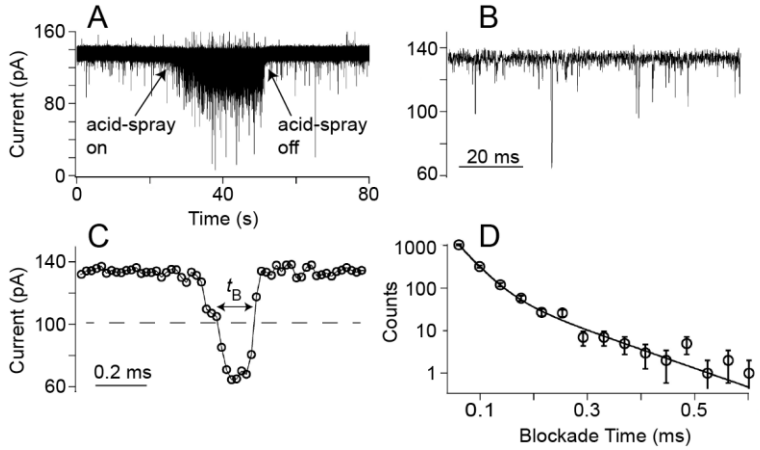

Figure S6: Spraying acidic solution on a trapped particle yields rapid protonation/deprotonation-induced fluctuations. (A) A single *p*-MBA particle is trapped in the pore in a pH 8 solution and a micropipette tip filled with matching electrolyte at pH 5 is positioned nearby and sprayed onto the pore creating short-lived downward current spikes. (B) The zoomed-in view of the current trace shows the time between protonation events is on the order of 10 ms. (C) Further zooming in shows the duration of each spike is on the order of 100 μs. The dashed line indicates the threshold level below which an event is logged. (D) The distribution of deprotonation times, t_B, is fit with a double exponential function (solid line) having mean blockade times τ_{fast} = (0.029 ± 0.002) ms and τ_{slow} = (0.098 ± 0.016) ms. These blockade times are consistent with previously reported deprotonation rates from carboxylic acid in an αHL nanopore (≈ 40 μs).[12] The blockade time distribution was calculated from 2 pores, 5 particles, 11 spray ejections and 1624 downward current fluctuation events. Data was collected under a 70 mV applied transmembrane potential in 3M KCl.

We hypothesize that these downward spikes correspond to protonation/deprotonation events, because the kinetics associated with them are consistent with a previous report that measured the deprotonation rate from amino acid residues in a wild-type αHL pore (t_{off} ~40 μs).[12] From the estimated frequency of short current blockades (k_{on} = (150 ± 50) s^{-1}) and the estimated pH inside the pore during the spraying step (pH ~ 5.4, see below), we calculate the average nanoparticle pK_a to be ca. 3.3 ± 0.5, which is in reasonable agreement with the pK_a for free *p*-MBA (pK_a = 4.16).[11] This shows that the trapped cluster can be used to detect protonation/deprotonation kinetics from the cluster-bound ligands and more importantly, that these kinetics are much faster than the kinetics seen for the longer-time discrete current state steps. Thus ruling out the possibility that the discrete current steps are connected to protonation/deprotonation events.

To estimate the pH in the pore during the spraying step we note that when we spray cluster solutions near the pore, we observe a slight reduction in the transmembrane current. This is because the ionic strength of the solution in and around the pore is reduced in the presence of the cluster solution, which has a lower KCl concentration ([KCl] = 2.4 M) than the surrounding bulk solution ([KCl] = 3M). Typical spraying leads to a ~5% reduction in the open pore current and we use this to estimate the relative contributions of the bulk and tip solutions inside the pore. Specifically, a 5% reduction in current indicates an effective ionic strength of [KCl] = 2.75M inside the pore. This means that the relative contributions of the bulk *x* and tip solutions *y* are described by the linear system of equations,

$$\begin{aligned} 3x + 2.4y &= 2.75 \\ x + y &= 1 \end{aligned} \qquad \text{(S3.1)}$$

From which we find $x = 0.6$ and $y = 0.4$.

Assuming this same ratio of spray to bulk solutions during the acidic spray experiment, and noting that the bulk solution pH = 8 while the acidic spray solution pH = 5, leads to the following expression for the pH inside the pore during the spraying step,

$$\begin{aligned} \left[H^+\right] &= 0.4\times10^{-5} + 0.6\times10^{-8} = 4.3\times10^{-6} \\ \text{pH} &= -\log\left(4.3\times10^{-6}\right) = 5.4 \end{aligned} \qquad \text{(S3.2)}$$

IV. Polarity dependence of PEG-capped particle blockades

It was stated in the main article that the S-PEG$_7$ ligands are positively charged in high ionic strength KCl. This is because PEG weakly binds K^+ cations, which makes the PEG behave like a polycation.[13] This remains true for the cluster bound PEG as well. Figure S7 below illustrates this fact by comparing S-PEG$_7$-capped particle current traces through a nanopore at +70 mV and -70 mV applied transmembrane potential. Recall that electrical ground is fixed on the *cis*-side of the pore and the PEG-capped particles are sprayed into the *cis*-side region. This means the reported asymmetry in the current blockades proves that the PEG acts like polycations making the nanoparticles behave as positively charged particles. In addition, zooming in on the current trace between particle blockade events shows that the free S-PEG$_7$ blockades show a greater on-rate to the pore under the negative applied potential. This verifies that the free PEG behaves like a cationic polymer.

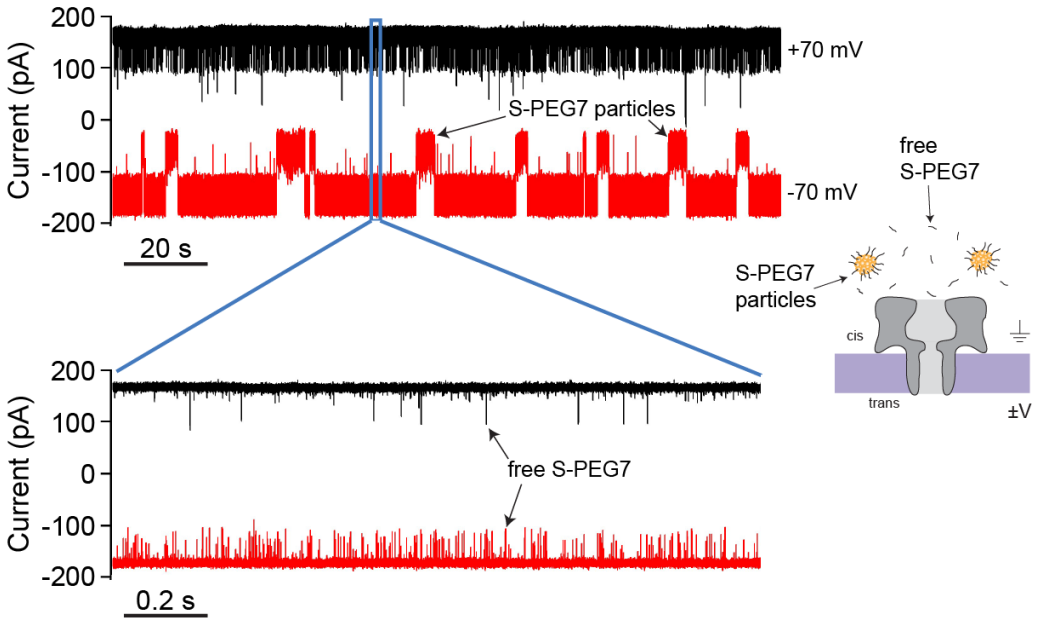

Figure S7: S-PEG$_7$-capped particles behave like cationic particles as evidenced by the asymmetry in the blockades under positive (black) and negative (red) applied voltage. (Top) A steady stream of PEG-capped particles ejected near the pore only yields long-time particle blockades in the negative voltage state. This shows that the particles are positively charged. (Bottom) A zoomed-in view of the current shows the shallow and short-lived blockades that arise from free S-PEG$_7$ interactions with the pore. These "free-PEG" blockades are more frequent in the negative voltage state, which is consistent with a previous report[13] that shows K^+ cations weakly bind to PEG thus making PEG behave like a polycation in high ionic strength KCl solutions. The inset cartoon serves to remind the reader about the voltage orientation with respect to the pore. Data shown here was taken at +70 mV (Black) and -70 mV (Red) in 3M KCl solution at pH 8.

V. References

1. Bertino, M. F.; Sun, Z. M.; Zhang, R.; Wang, L. S. Facile syntheses of monodisperse ultrasmall Au clusters. *J. Phys. Chem. B*, **2006**, *110*, 21416.

2. Song, L.; Hobaugh, M. R.; Shustak, C.; Cheley, S.; Bayley, H.; Gouaux, J. E. Structure of staphylococcal α-Hemolysin, a heptameric transmembrane pore. *Science*, **1996**, *274*, 1859.

3. Angevine, C. E.; Chavis, A. E.; Kothalawala, N.; Dass, A.; Reiner, J. E. Enhanced single molecule mass spectrometry via charged metallic clusters. *Anal. Chem*. **2014**, *86*, 11077.

4. Shi, W.; Friedman, A. K.; Baker, L. A. Nanopore sensing. *Anal. Chem*., **2017**, *89*, 157.

5. Angevine, C. E.; Seashols-Williams, S. J.; Reiner, J. E. Infrared laser heating applied to nanopore sensing for DNA duplex analysis. *Anal. Chem*., **2016**, *88*, 2645.

6. Bhattacharya, S.; Muzard, J.; Payet, L.; Mathe, J.; Bockelmann, U.; Aksimentiev, A.; Viasnoff, V. Rectification of the current in a α-Hemolysin pore depends on the cation type: The alkali series probed by molecular dynamics simulations and experiments. *J. Phys. Chem. C*, **2011**, *115*, 4255.

7. Raillon, C.; Granjon, P.; Graf, M.; Steinbock, L. J.; Radenovic, A. Fast and automatic processing of multi-level events in nanopore translocation experiments. *Nanoscale*, **2012**, *4*, 4916.

8. DeBlois, R. W.; Bean, C. P. Counting and sizing of submicron particles by the resistive pulse technique. *Rev. Sci. Instrum*., **1970**, *41*, 909.

9. Ackerson, C. J.; Jadzinsky, P. D.; Kornberg, R. D. Thiolate ligands for synthesis of water-soluble gold clusters. *J. Am. Chem. Soc*., **2005**, *127*, 6550.

10. Li, R.; Haiming, Lv.; Zhang, X.; Liu, P.; Chen, L.; Cheng, J.; Zhao, B. *Spectrochim. Acta A Mol. Biomol. Spectrosc*., **2015**, *148*, 369.

11. Koivisto, J.; Chen, X.; Donnini, S.; Lahtinen, T.; Hakkinen, H.; Groenhof, G.; Pettersson, M. Acid-base properties and surface charge distribution of the water-soluble $Au_{102}(p\text{MBA})_{44}$ nanocluster. *J. Phys. Chem. C*. **2016**, *120*, 10041.

12. Kasianowicz J. J.; Bezrukov, S. M. Protonation dynamics of the alpha-toxin ion channel from spectral analysis of pH-dependent current fluctuations. *Biophys. J*., **1995**, *69*, 94.

13. Reiner, J. E.; Kasianowicz, J. J.; Nablo, B. J.; Robertson, J. W. F. Theory for polymer analysis using nanopore-based single-molecule mass spectrometry. *Proc. Natl. Acad. Sci. USA*, **107**, 2010, 12080.